GEOLOGICAL SURVEY OF CANADA
OPEN FILE 7852

Targeted Geoscience Initiative 4: Contributions to the Understanding of Precambrian Lode Gold Deposits and Implications for Exploration

Depositional setting of Algoma-type banded iron formation from the Meadowbank, Meliadine, and Musselwhite gold deposits

Blandine Gourcerol[1], Phillip C. Thurston[1], Daniel J. Kontak[1], Olivier Côté-Mantha[2], and John Biczok[3]

[1]Laurentian University, Sudbury, Ontario
[2]Agnico Eagle Mines Ltd., Val d'Or, Quebec
[3]Goldcorp Canada Ltd., Thunder Bay, Ontario

2015

Recommended citation

Gourcerol, B., Thurston, P.C., Kontak, D.J., Côté-Mantha, O., and Biczok, J., 2015. Depositional setting of Algoma-type banded iron formation from the Meadowbank, Meliadine, and Musselwhite gold deposits, *In:* Targeted Geoscience Initiative 4: Contributions to the Understanding of Precambrian Lode Gold Deposits and Implications for Exploration, (ed.) B. Dubé and P. Mercier-Langevin; Geological Survey of Canada, Open File 7852, p. 55–68.

Publications in this series have not been edited; they are released as submitted by the author.

Contribution to the Geological Survey of Canada's Targeted Geoscience Initiative 4 (TGI-4) Program (2010–2015)

TABLE OF CONTENTS

Depositional setting of Algoma-type banded iron formation from the Meadowbank, Meliadine, and Musselwhite gold deposits

Blandine Gourcerol[1]*, Phillip C. Thurston[1], Daniel J. Kontak[1],
Olivier Côté-Mantha[2], and John Biczok[3]

[1]Mineral Exploration Research Centre, Laurentian University, Sudbury, Ontario, P3E 2C6
[2]Agnico Eagle Mines Ltd. – Division Exploration, 765 Chemin de la mine Goldex, Val-d'Or, Quebec, J9P 4N9
[3]Goldcorp Canada Ltd., Musselwhite Mine, P.O. Box 7500, Thunder Bay, Ontario, P7B 6S8
*Corresponding author's e-mail: gourcerol.blandine@gmail.com

ABSTRACT

Algoma-type banded iron formations (BIFs) are chemical sedimentary rocks in Archean greenstone belts that comprise alternating layers of iron-rich minerals and chert and are generally interstratified with bimodal submarine volcanic rocks. However, the geological setting for Algoma-type BIF deposition remains equivocal due to the overprinting effects of post-depositional deformation and metamorphism, and the absence of modern analogues for comparative studies. Recent studies suggest the abundance of rare earth elements and yttrium (REE+Y) in chert bands may reflect the primary BIF geochemical signature and therefore may constrain geological settings favourable for BIF deposition.

In this study, the results of LA-ICP-MS analysis of chert at three BIF-hosted gold deposits are presented to assess whether epigenetic gold mineralization is preferentially developed within a particular geochemical type of BIF. Three deposits were studied: 1) the Meadowbank deposit (Churchill Province); 2) the Meliadine gold district (Churchill Province); and 3) the Musselwhite deposit (Superior Province). The results of this study, which explores REE and yttrium as tracers of depositional processes for Algoma-type BIF, suggest that chert bands record either (1) interaction of seawater with Fe-oxyhydroxides, as suggested by heavy REE enrichment coupled with La and Y enrichment; (2) high-temperature (>250ºC) hydrothermal fluids, as suggested by positive Eu excursions; and/or (3) hydrogeneous contamination, which is suggested by relatively consistent REE concentrations and a chondritic Y/Ho ratio. Moreover, the pH conditions of the water column at the time of BIF deposition are evaluated using Ce/Ce* as a pH proxy, with acidic conditions associated with positive Ce/Ce* anomalies. This data set does not suggest there is a chemical preference of the studied BIF for epigenetic gold mineralization.

INTRODUCTION

Algoma-type banded iron formation (BIF) is thinly bedded, chemical sedimentary rocks comprising alternating layers of iron-rich minerals and chert. These rocks are typically intercalated with Eoarchean to late Paleoproterozoic volcano-sedimentary sequences within greenstone belts (Goodwin, 1973; Bekker et al., 2010). Based on their sedimentary and geochemical features, a restricted basin under the influence of seawater and hydrothermal vent fluids is one potential BIF depositional setting (e.g. Bolhar et al., 2005; Ohmoto et al., 2006). In this model, the iron-rich minerals precipitated contemporaneously with hydrothermal vent fluids to form siderite and various iron oxyhydroxides. These primary minerals are diagenetically transformed to hematite, magnetite, iron silicates, and sulphides, which characterize the type BIF mineral assemblage. The interbedded chert horizons are considered to reflect (1) periods of hydrothermal quiescence; (2) a temporary decrease in the contribution of the hydrothermal fluid (Bolhar et al., 2005; Thurston et al., 2011); (3) hydrothermal precipitates from vent fluids (Allwood et al., 2010; Thurston et al., 2011); and/or (4) the products of secondary replacement (Hanor and Duchac, 1990).

In this study, we explore the chert geochemistry at three BIF-hosted gold deposits (the ~4 Moz Au Meadowbank deposit, hosted by the 2.71 Ga Woodburn Lake greenstone belt; the ≥2.8 Moz Au Meliadine district, hosted by the 2.6 Ga Ennadai-Rankin greenstone belt; and the ~6 Moz Au Musselwhite deposit, hosted by the 2.9–3 Ga North Caribou greenstone belt; Fig. 1). The BIFs at each of these deposits are either intercalated with mafic to ultramafic volcanic rocks or associated interflow sediments. These three gold deposits were selected to validate and refine the restricted-basin

Gourcerol, B., Thurston, P.C., Kontak, D.J., Côté-Mantha, O., and Biczok, J., 2015. Depositional setting of Algoma-type banded iron formation from the Meadowbank, Meliadine, and Musselwhite gold deposits, *In:* Targeted Geoscience Initiative 4: Contributions to the Understanding of Precambrian Lode Gold Deposits and Implications for Exploration, (ed.) B. Dubé and P. Mercier-Langevin; Geological Survey of Canada, Open File 7852, p. 55–68.

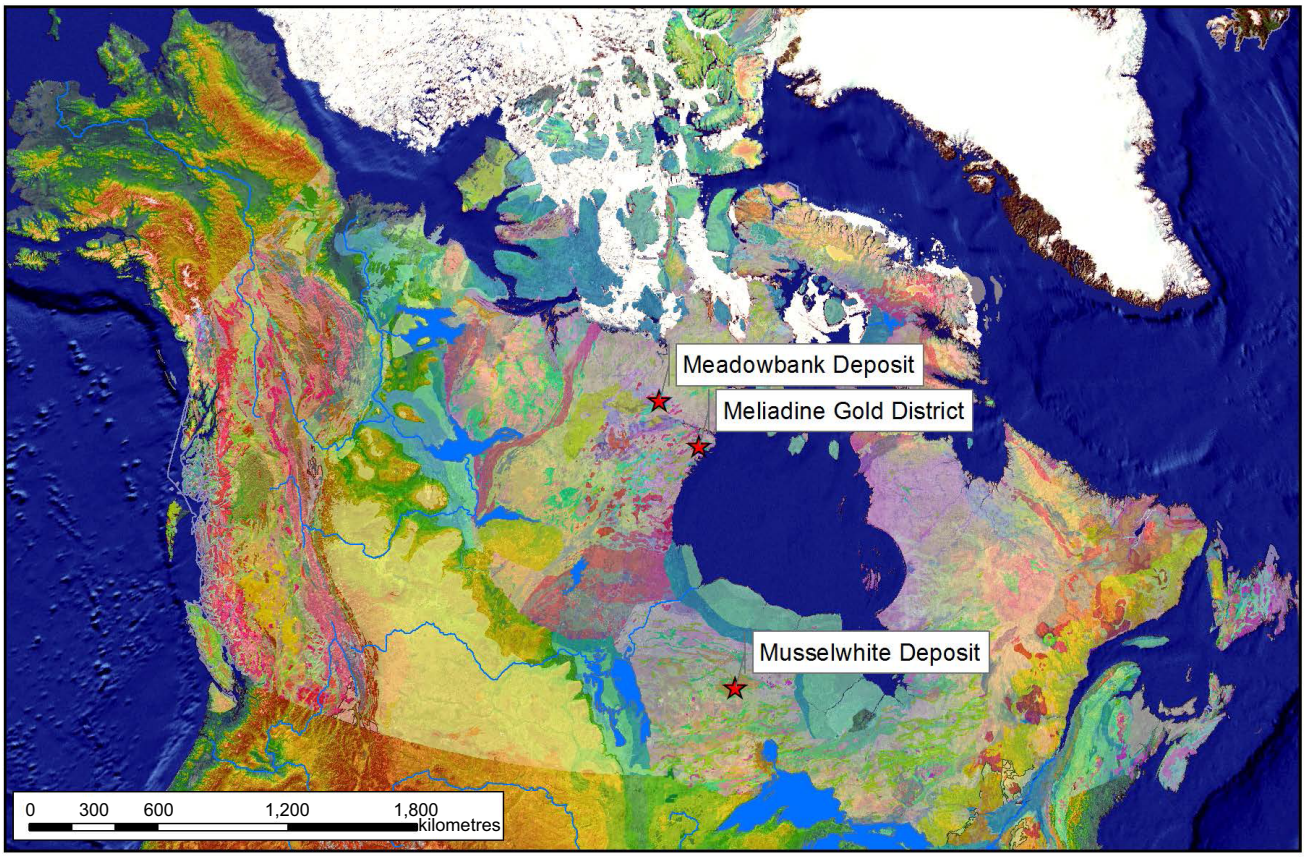

Figure 1. Localization of the three deposits investigated in this study. The Meadowbank deposit and the Meliadine gold district are within the Churchill Province, west of Hudson Bay; the Musselwhite deposit is within the Superior Province, south of Hudson Bay (after Wheeler et al., 1996).

model as a depositional setting for Algoma-type BIFs by using the geochemical signature of the chert bands as a proxy for the primary signature of ocean water chemistry and hydrothermal vent fluids. In detail, this hypothesis was tested by (1) defining the role of chemical reservoirs (i.e. seawater, hydrothermal fluids, and terrestrial detritus) in chert deposition; and (2) using redox-sensitive rare earth elements (REE) + Y to assess the oxygenation state of the water column during chert precipitation.

ANALYTICAL METHODS AND DATA TREATMENT

The BIF samples collected for the study included (1) 37 samples from drillcore and outcrops from the Meadowbank deposit (i.e. West IF, Central BIF, East BIF); (2) 40 samples in the Meliadine deposit area (i.e. Pump, F-Zone, and Discovery); and (3) 23 samples from the Musselwhite deposit (i.e. chert-magnetite (4B), garnet-grunerite-(chert) (4EA), garnetiferous amphibolite (4E), and garnet-biotite schist (4F) facies) (Fig. 1). Polished thin sections (100 µm thick) were examined, using both transmitted and reflected light microscopy, and selected material was studied in more detail using the scanning electron microscopy with X-ray microanalysis (SEM-EDS) to select the chert bands with minimal amounts of detrital mineral inclusions and other contaminants related to alteration, diagenesis, metamorphic, or ore-forming events.

The trace element and REE analyses of the chert were obtained using a Resonetics Resolution M-50 laser ablation instrument coupled to a Thermo X-Series II quadrupole inductively coupled plasma mass spectrometry (ICP-MS) at the Geochemical Fingerprinting Laboratory at Laurentian University, Sudbury, Ontario following the protocol of Kamber and Webb (2007). As chert bands have very low concentration of REE, spot analyses may be below the limit of detection for many elements. Thus, in order to circumvent this issue, line traverses using both 140 and 190 µm beam diameters with a repetition rate of 10 Hz and an energy density of 7 J/cm^2 were used to obtain data that is above the detection limit. However, the line traverse method increases the influence of any detrital contaminants, either as inclusions or minerals disseminated along the traverse line. Therefore, the Queensland alluvial shale composite (MUQ) was used to normalize the REE+Y values to attenuate the influence of potential terrigenous input. The MUQ composition represents a mixed bimodal felsic and mafic volcanic provenance (Kamber

Table 1. Estimated detection limits for elements and rare earth elements referred to in this study.

Element	Estimated LOD (ppm)	Element	Estimated LOD (ppm)	Element	Estimated LOD (ppm)
Li	0.011	Y	0.006	Pb	0.004
Be	0.086	Zr	0.010	Th	0.005
Si	43.522	Nb	0.007	U	0.003
Sc	0.025	Mo	0.035	Ho	0.004
Ti	0.072	Ag	0.005	Er	0.012
V	0.007	Cd	0.071	Tm	0.004
Cr	0.111	In	0.005	Yb	0.016
Mn	0.062	Sn	0.006	Lu	0.003
Fe	0.202	Er	0.012	Hf	0.011
Co	0.005	Tm	0.004	Ta	0.004
Ni	0.050	Yb	0.016	W	0.016
Cu	0.042	Lu	0.003	Au	0.015
Zn	0.021	Hf	0.011	Tl	0.002
Ga	0.007	Ta	0.004	Pb	0.004
As	0.028	W	0.016	Th	0.005
Rb	0.004	Au	0.015	U	0.003
Sr	0.005	Tl	0.002		

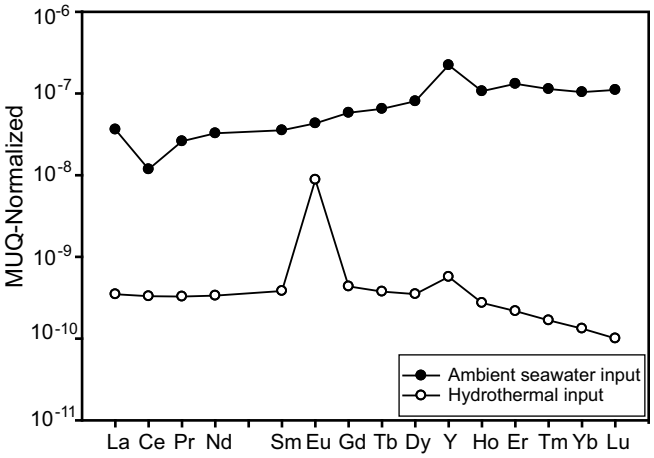

Figure 2. Upper crust MUQ-normalized REE patterns illustrating the chemical signatures of the two modern settings relevant to this study: ambient seawater and hydrothermal vent fluid (data from Bau and Dulski, 1996).

et al., 2005), which acts as a proxy for the expected average terrigenous input from a typical bimodal greenstone belt into the Archean ocean (e.g. Bolhar et al., 2005; Thurston et al., 2011).

The elemental concentrations reported in this study represent the integrated signal over the length of the traverse. The element list used for each analysis included the 14 REEs in addition to Li, Be, Si, Sc, Ti, V, Cr, Mn, Fe, Co, Ni, Cu, Zn, Ga, As, Rb, Sr, Zr, Nb, Mo, Ag, Cd, In, Sn, Sb, Cs, Ba, Hf, Ta, W, Tl, Pb, Th, and U. The NIST 612 glass standard was analysed at the beginning and at the end of each line traverse. The data interpretation presented below focuses on samples that yielded REE concentrations that are consistently above the analytical detection limits (Table 1).

RARE-EARTH AND YTTRIUM SYSTEMATICS

The presence and abundance of REE+Y in chert bands may represent a primary signature, which can be influenced by one or more processes: 1) precipitation from open marine seawater (e.g. Bau and Dulski, 1996); 2) precipitation from vent-sourced hydrothermal fluids (e.g. Danielson et al., 1992; Allwood et al., 2010); and 3) chemical inheritance due to replacement of primary BIF minerals (e.g. Hanor and Duchac, 1990). Chert geochemistry is also strongly dependent on the extent of terrigenous detritus (Alexander et al., 2008) and oceanographic processes (e.g. phosphate circulation and precipitation).

Several studies have shown that the REE+Y systematics of Archean seawater is analogous to the modern ocean (Fig. 2; e.g. Bau and Dulski, 1996; Lawrence and Kamber, 2006; Thurston et al., 2011). It follows, therefore, that the shale (i.e. MUQ) normalized REE+Y pattern from the Archean seawater will be characterized by (1) a depletion in light rare earth elements (LREE) relative to heavy rare earth elements (HREE); (2) a super-chondritic Y/Ho ratio (i.e. >27), yielding a positive Y/Y^*_{MUQ} anomaly, commonly between 40 and 90; and (3) a slightly positive La anomaly (La/La^*_{MUQ} between 1.15 and 1.3). Moreover, as the chemistry of Archean seawater was also influenced by volcanism, water-rock interaction (Veizer, 1988), and the contribution of high-temperature (>250ºC) hydrothermal fluids (Fig. 2; Bau and Dulski, 1996; Kamber et al., 2004), these processes are characterized by variable, but well developed positive Eu anomalies (Fig. 2; Kamber et al., 2004).

Metamorphism and ore-forming processes (i.e. epigenetic fluids) may remobilize REE+Y and consequently alter the primary signature of chert bands. Therefore, the REE+Y signature of seawater and hydrothermal vent fluids will not be detected in MUQ-normalized profiles, as this paper addresses, thus a careful selection of samples was done prior to analytical studies.

DISCUSSION

Rare Earth and Yttrium Systematic Characteristics

Meadowbank Area

Data for chert samples from the Central BIF, East BIF, and West IF within the Meadowbank area (Gourcerol et al., 2014) show relatively uniform REE+Y patterns that include a slight to moderate enrichment in HREE, relative to LREE and MREE (Nd/Yb_{MUQ} = 0.05–0.54), that are associated with slight to moderate positive La, Y, and Eu anomalies (La/La^*_{MUQ} = 0.89–4.65, Y/Y^*_{MUQ} = 0.88–1.96, Eu/Eu^*_{MUQ} = 1.25–5.12) and super-chondritic to chondritic Y/Ho values (Y/Ho = 24.2–53.72) (Fig. 3). These observations record the

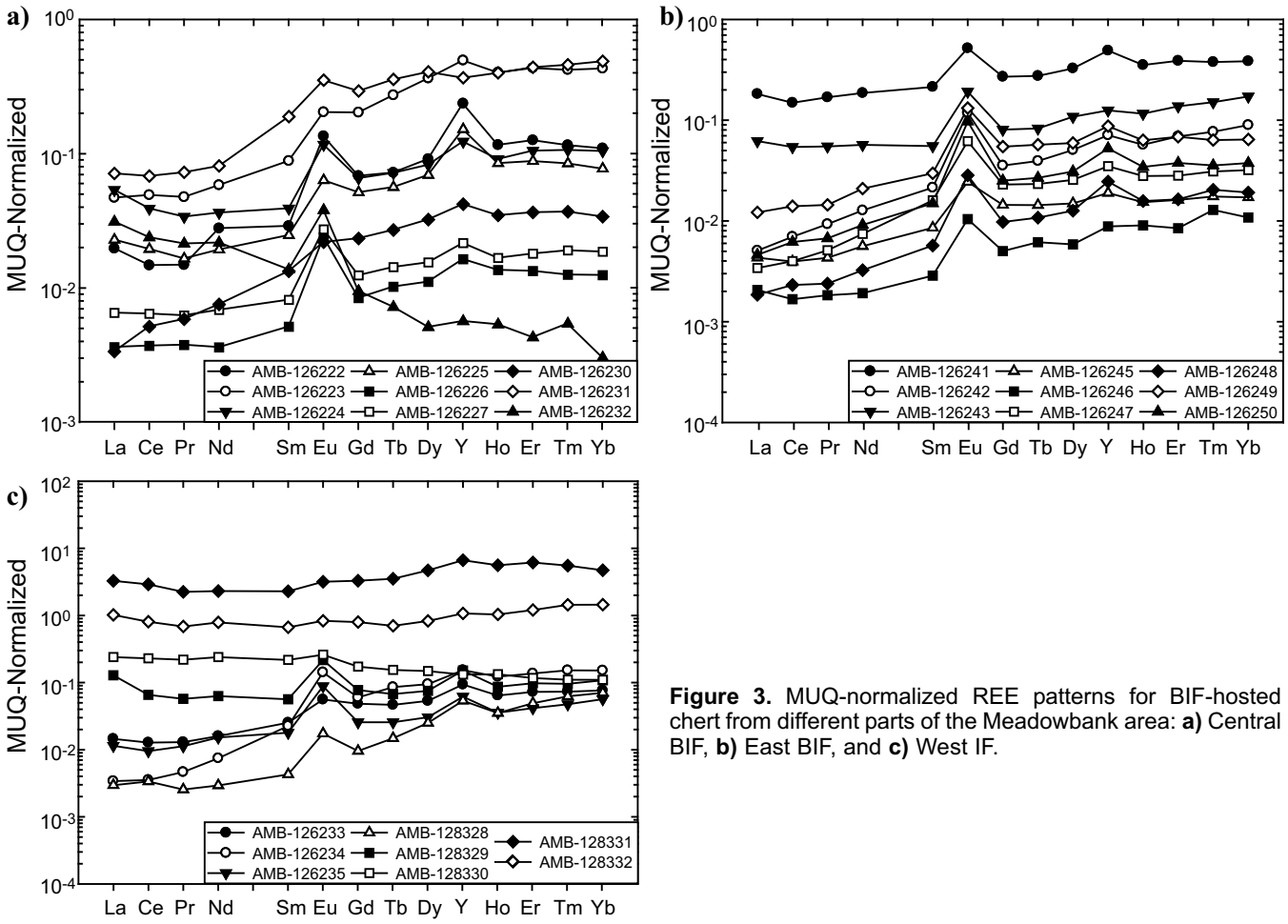

Figure 3. MUQ-normalized REE patterns for BIF-hosted chert from different parts of the Meadowbank area: **a)** Central BIF, **b)** East BIF, and **c)** West IF.

influence of ambient seawater and high-temperature (>250ºC) hydrothermal fluids during chert deposition. Some of the notable departures of the data from the expected pattern are discussed below and in this context we note that enrichments in particular elements serve as proxies for other influences: Sr for C and hence apatite, Ga for Al and thus detritus, and Zr for zircon (representing felsic ash), all of which are confirmed by petrographic study.

A group of samples from the East BIF (samples AMB-126241 and AMB-126243; Fig. 3b) and the West IF (samples AMB-128330, AMB-128331, and AMB-128332; Fig. 3c) show relatively flat REE patterns (Pr/Sm_{MUQ} = 0.79–1.03) associated with chondritic Y/Ho values (Y/Ho = 26.02–36.71). Enrichments in Sr (i.e. 27.9–55 ppm, Fig 3b; and 64.9–1090 ppm, Fig. 2c), Zr (i.e. 0.97–2.17 ppm, Fig. 3b; and 19.1–43.4 ppm, Fig. 3c), and variable amounts of Th (i.e. 1.055–4.2 ppm, Fig. 3c) and Ga (i.e. 16.04–27.8 ppm, Fig. 3c) relative to the bulk of samples is illustrated for most of samples from the West IF. Two samples from the Central BIF (samples AMB-126223 and AMB-126231; Fig. 3a) show depletion in LREE relative to HREE, but moderate to flat patterns for the MREE and HREE, which are associated with chondritic Y/Ho values (Y/Ho = 24.2–32.41) and enrichment in Zr (i.e. 104.9–183 ppm), Ga (i.e. 6.83–141.4 ppm), Sr (i.e. 20.4–95.2 ppm), and Th (i.e. 1.22–7.7 ppm). These numbers suggest variable amounts of detrital contamination during chert deposition. The presence of apatite in chert bands from different BIFs, as revealed in SEM images, could explain the elevated Sr values, as it is a proxy for Ca, and suggests, therefore, that the West IF chert chemistry is more affected by sulphate (apatite) deposition. Moreover, zircon and monazite were seen in SEM images of samples AMB-126223 and AMB-126231, which may account for the strong enrichment in Zr and anomalous HREE enrichment in chert from the Central BIF.

Meliadine Gold District

Data for chert samples from the Pump, F-Zone, and Discovery deposits within the Meliadine gold district yield variable REE+Y patterns (Fig. 4). Chert samples at Pump yield LREE-depleted patterns (Nd/Yb_{MUQ} = 0.06–0.75), sub-chondritic to chondritic Y/Ho values (Y/Ho = 11.44–32.53), variable La and Y concentrations (La/La^*_{MUQ} = 0.08–1.11, Y/Y^*_{MUQ} = 0.54–1.13), and positive Eu anomalies (Eu/Eu^*_{MUQ} = 2.17–6.13) (Fig. 4a). These results suggest that chert precipitated

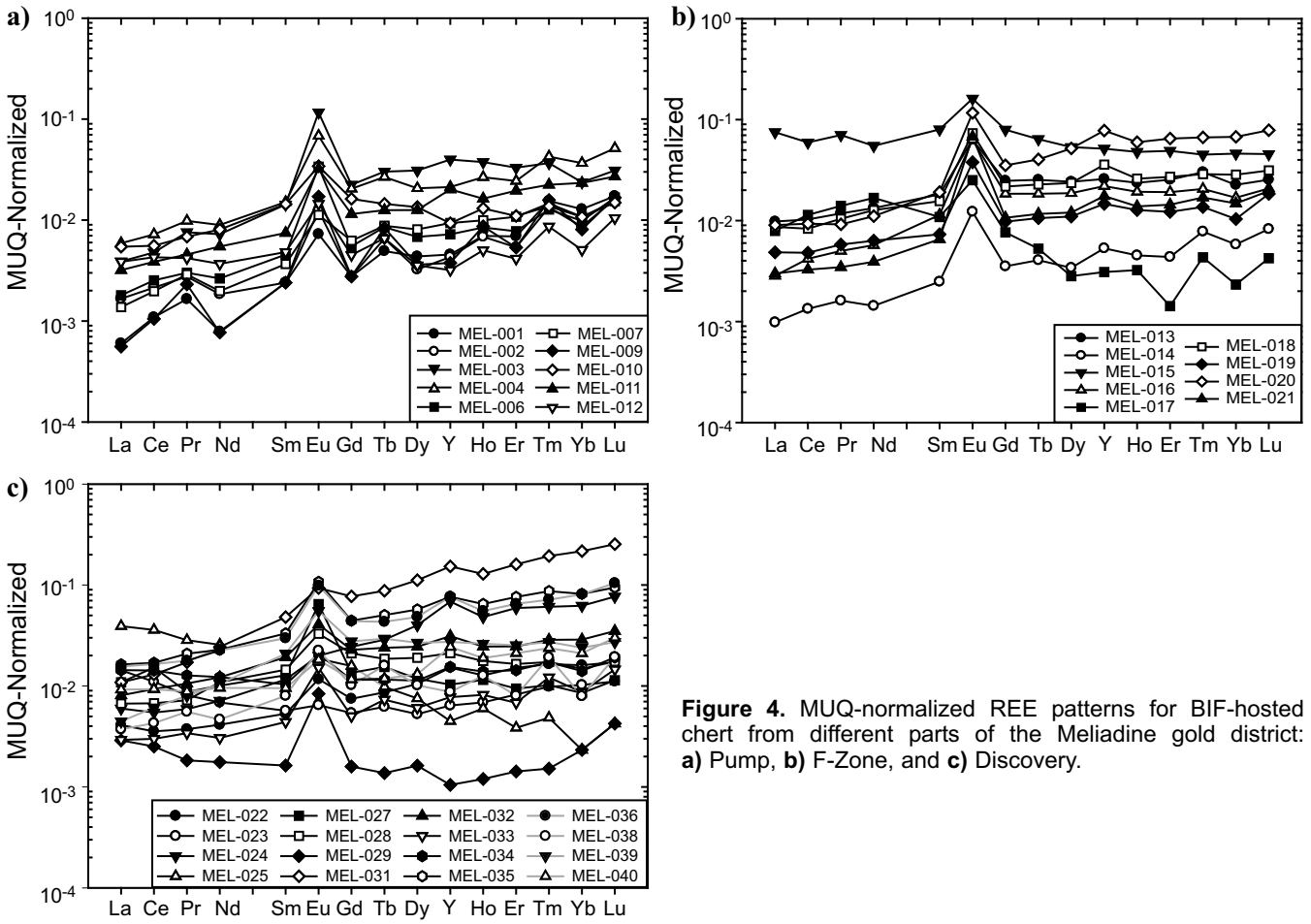

Figure 4. MUQ-normalized REE patterns for BIF-hosted chert from different parts of the Meliadine gold district: **a)** Pump, **b)** F-Zone, and **c)** Discovery.

from high-temperature (>250ºC) hydrothermal vent fluids. The Y/Ho ratios for most of the samples are lower than chondritic values (i.e. 27) and correspond with negative La and Y anomalies, which together represent compositions that are unlike that of modern ocean water.

All chert samples at F-Zone show LREE-depleted patterns (Nd/Yb_{MUQ} = 0.16–0.59). In detail, samples MEL015 and MEL017 yield slightly anomalous HREE-depleted concentrations (Nd/Yb_{MUQ} = 1.19–7.21) and slightly to strongly enriched La, Y, and Eu concentrations (La/La^*_{MUQ} = 1.00–1.43, Y/Y^*_{MUQ} = 1.05–1.35, Eu/Eu^*_{MUQ} = 2.12–8.14; Fig. 4b). These trace-element patterns are characteristic of high-temperature (>250ºC) hydrothermal vent fluids and/or seawater. In contrast, all samples yield chondritic Y/Ho values (Y/Ho = 25.25–36.34) and Sr enrichment (i.e. 6.5–30.6 ppm) that suggest detrital input and possible primary apatite grains.

Chert samples from the Discovery deposit are LREE-depleted (Nd/Yb_{MUQ} = 0.11–0.87) (N.B. except sample MEL-027: Nd/Yb_{MUQ} = 12.89) (Fig. 4c). Slight to moderate La, Y, and Eu enrichments (La/La^*_{MUQ} = 0.69–2.1, Y/Y^*_{MUQ} = 0.80–1.28, Eu/Eu^*_{MUQ} = 1.05–7.46) are also typical of most samples (N.B. except for sample MEL-038: La/La^*_{MUQ} = 0.47, Y/Y^*_{MUQ} = 0.85, Eu/Eu^*_{MUQ} = 2.13) (Fig. 4c). The Y/Ho ratios vary from sub-chondritic to chondritic (Y/Ho = 18.23–37.48). These chemical features are typical of an input of seawater and/or high-temperature (>250ºC) hydrothermal vent fluids during chert deposition. Most of the samples exhibit chondritic Y/Ho values associated with Sr enrichment (i.e. 0.3–177 ppm) and moderate Ga enrichment (i.e. 1.32–7.04 ppm). In contrast, samples MEL-038, MEL-039, and MEL-040 yield trace-element concentrations (± elevated Ca) that are consistent with detrital contamination. Sample MEL-038 yielded elevated Y/Ho ratios that correspond to depletion in La and Y concentrations, which was also reported for some chert samples from the Pump deposit.

Musselwhite Area

Data for chert samples from the chert-magnetite (4B facies; Fig. 5a), the garnetiferous amphibolite (4E facies; Fig. 5b), the garnet-grunerite-(chert) (4EA facies; Fig. 5c), and the garnet-biotite schist (4F facies; Fig. 5f) within the Musselwhite area were reported by Gourcerol et al. (2015). These samples exhibit rela-

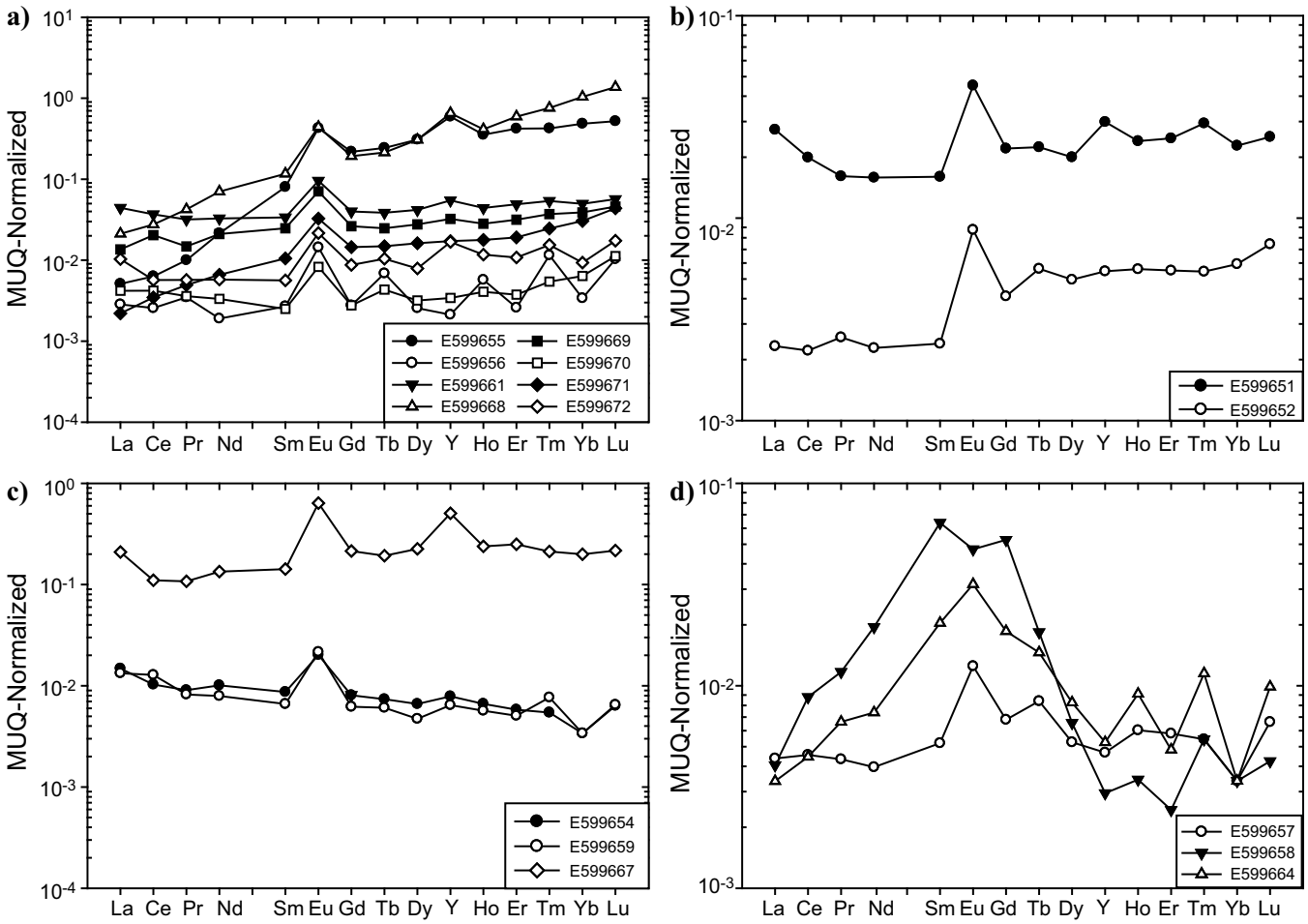

Figure 5. MUQ-normalized REE patterns for chert samples from BIFs in different parts of the Musselwhite area: **a)** unit 4B — oxide-dominant facies samples, **b)** unit 4E — garnetiferous amphibolite samples, **c)** unit 4EA — garnet-grunerite samples, excluding samples E599660, E599665, and E599666, and **d)** unit 4F — biotite-garnet schist samples.

tively uniform REE+Y patterns, except for the 4F facies (Fig. 5d). Most chert sampled from the 4B facies are HREE enriched (Nd/Yb_{MUQ} = 0.04–0.66), yield slight to moderate positive La, Y, and Eu anomalies (La/La^*_{MUQ} = 0.8–1.49, Y/Y^*_{MUQ} = 0.87–1.49, Eu/Eu^*_{MUQ} = 2.6–3.61), and chondritic Y/Ho values (Y/Ho = 22.13–44.01) (Fig. 5a). These concentrations may record seawater and/or high-temperature (>250ºC) hydrothermal vent fluids during chert deposition. Variable detrital input is also suspected based on the chondritic Y/Ho values. Sample E599656 differs from the majority of samples by its negative La and Y anomalies (La/La^*_{MUQ} = 0.21, Y/Y^*_{MUQ} = 0.51) and very low Y/Ho value (i.e. 9.79), which could reflect precipitation of chert under the influence of high-temperature (>250ºC) hydrothermal vent fluid with variable seawater input. It should be noted that samples E599655 and E599668 are Sr-enriched, (i.e. 848.8 ppm and 150.8 ppm, respectively), which may be due to the presence of carbonate minerals in the chert. The presence of carbonate in the LA-ICP-MS traverse is illustrated by stronger depletion in LREE relative to HREE.

The two samples from the 4E facies show LREE depletion (Nd/Yb_{MUQ} = 0.39–0.7), are slightly to moderately La, Y, and Eu enriched (La/La^*_{MUQ} = 0.7–1.66, Y/Y^*_{MUQ} = 0.98–1.23, Eu/Eu^*_{MUQ} = 2.43–2.6), and yield super-chondritic to chondritic Y/Ho values (Y/Ho = 25.71–32.8) (Fig. 5b). These seem to record seawater, high-temperature (>250ºC) hydrothermal fluid and/or a minor detrital input during chert deposition.

The chert samples from 4EA facies are characterized by relatively flat to slightly fractionated patterns with LREE enrichment (Nd/Yb_{MUQ}= 0.39–0.7), except for samples E599654 and E599659 that show depleted HREE patterns LREE (i.e. Nd/Yb_{MUQ} = 1.51–2.04) and are associated with positive Eu anomalies (Eu/Eu^*_{MUQ} = 2.34–3.97) (Fig. 5c). Considering the La and Y anomalies and Y/Ho values, two groups of samples are present: (1) samples E599654, E599659, and E599667 show positive La and Y anomalies (La/La^*_{MUQ} = 1.51–3.02, Y/Y^*_{MUQ} = 1.2–2.07) and super-chondritic Y/Ho ratios (Y/Ho = 29.86– 55.91; Fig. 5c); and (2) samples E599660, E599665, and E599666 show negative La and Y anomalies

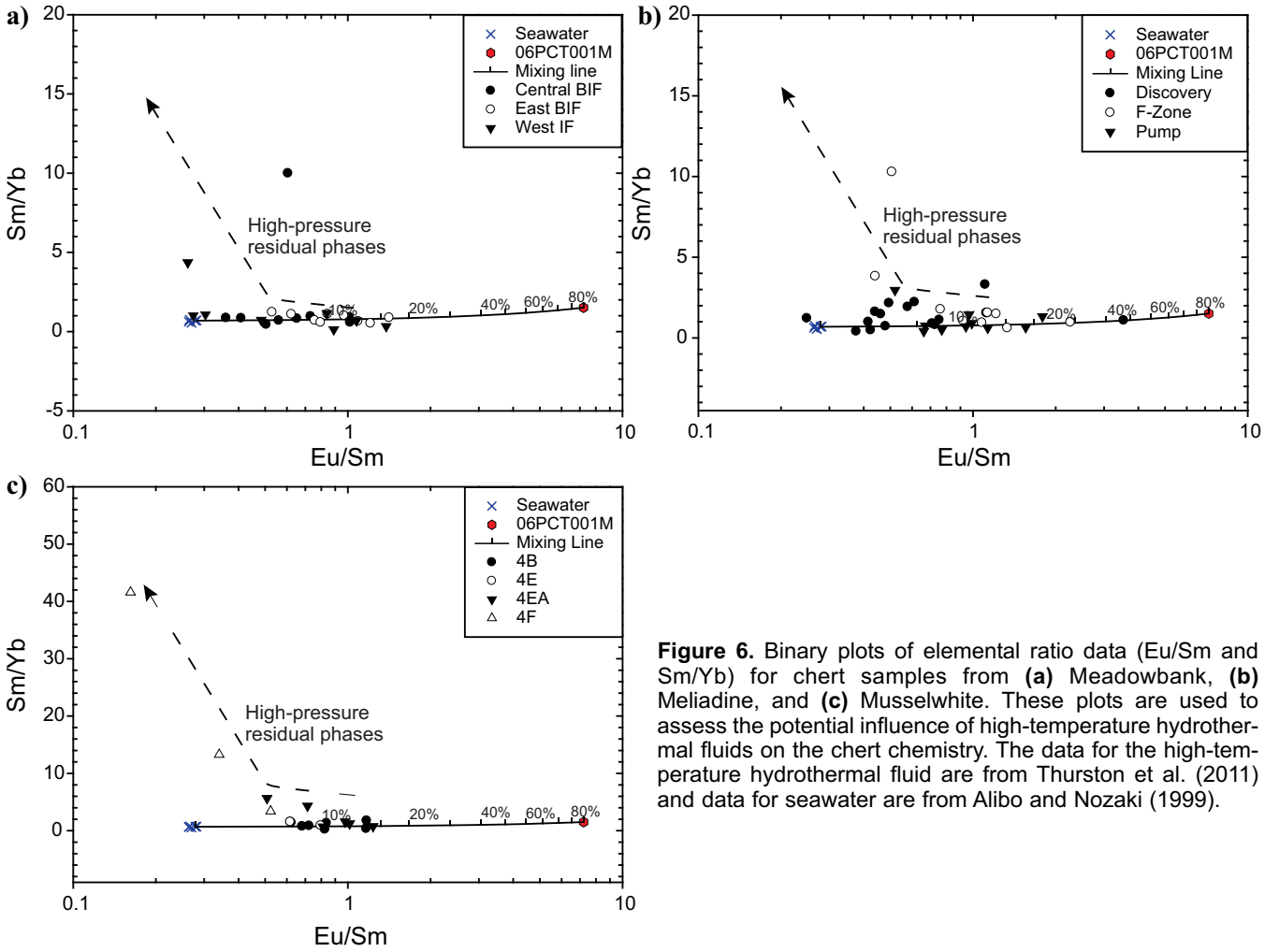

Figure 6. Binary plots of elemental ratio data (Eu/Sm and Sm/Yb) for chert samples from **(a)** Meadowbank, **(b)** Meliadine, and **(c)** Musselwhite. These plots are used to assess the potential influence of high-temperature hydrothermal fluids on the chert chemistry. The data for the high-temperature hydrothermal fluid are from Thurston et al. (2011) and data for seawater are from Alibo and Nozaki (1999).

(La/La^*_{MUQ} = 0.04–0.12, Y/Y^*_{MUQ} = 0.22–0.71) and very low Y/Ho ratios (Y/Ho = 4.11–16.52; Fig. 5c).

These results suggest that a seawater and/or high-temperature (>250ºC) hydrothermal vent-fluid component is recorded within chert bands for the first group of samples, whereas the second group likely precipitated from high-temperature (>250ºC) hydrothermal vent fluid with variable seawater influence, which is similar to the Meliadine samples.

The chert bands within the garnet-biotite schist (4F) facies are geochemically anomalous compared to chert at the other studied deposits. The former samples show variable, but elevated LREE and MREE enrichments (Pr/ Sm_{MUQ} = 0.18–0.83) and only moderately positive Eu anomalies (Eu/Eu^*_{MUQ} =1.08–1.94) are noted (Fig. 5d). This facies is distinguished from the others by its REE+Y signature and, furthermore, is similar to the argillite studied by Thurston et al. (2011), which documented only a weak hydrothermal-fluid influence.

Assessing the Influence of High-Temperature Hydrothermal Fluids

Most chert samples from Meadowbank, Meliadine, and Musselwhite show the influence of seawater and high-temperature (>250ºC) hydrothermal fluids. In this section, we calculate a binary mixing line between seawater and hydrothermal fluids in order to explore the relative importance of these fluids in chert deposition. The two end-members of this mixing line are represented in Figure 6: 1) seawater composition from the North Pacific (Alibo and Nozaki, 1999); and 2) an Archean hydrothermally precipitated chert sample (i.e. sample 06PCT001M; Thurston et al., 2011). Modern vent fluids were not used for mixing models due to geochemical differences between these fluids and Archean greenstone belt hydrothermal fluids (SiO_2-rich, Fe-poor, and highly alkaline fluids, which differ from the modern Fe-rich and acidic hydrothermal fluids; Shibuya et al., 2010).

Most of the samples in this study fall on the mixing line despite some samples exhibiting high Sm/Yb ratios (Fig. 6). The Sm/Yb ratio is particularly sensitive to high-pressure residual magmatic or metamorphic phases, such as amphibole and garnet, which may reflect the presence of some of these phases in chert bands derived from eroding source rocks during BIF formation.

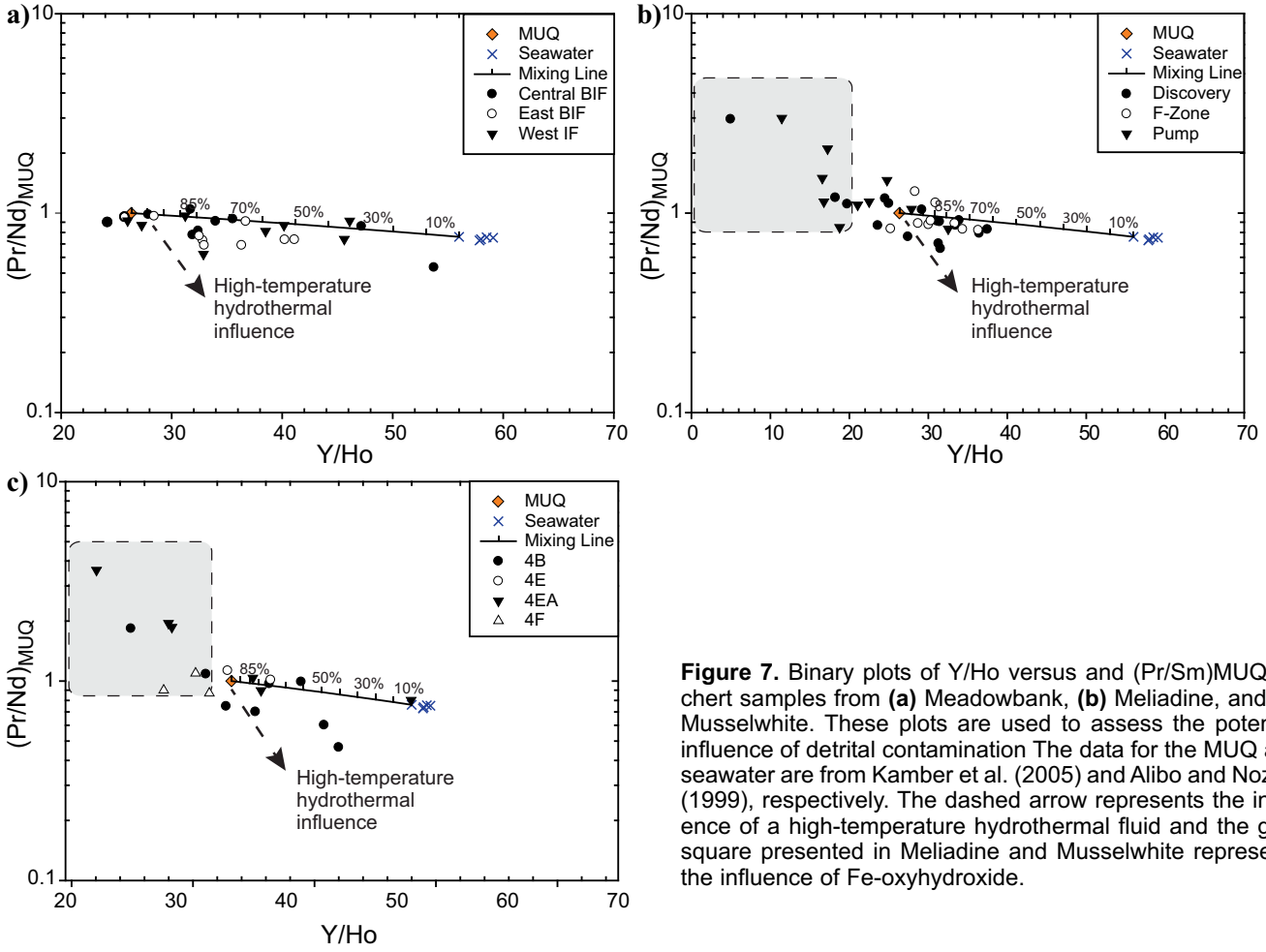

Figure 7. Binary plots of Y/Ho versus and (Pr/Sm)MUQ for chert samples from **(a)** Meadowbank, **(b)** Meliadine, and **(c)** Musselwhite. These plots are used to assess the potential influence of detrital contamination The data for the MUQ and seawater are from Kamber et al. (2005) and Alibo and Nozaki (1999), respectively. The dashed arrow represents the influence of a high-temperature hydrothermal fluid and the grey square presented in Meliadine and Musselwhite represents the influence of Fe-oxyhydroxide.

At Meadowbank, samples from the Central BIF suggest an input from the high-temperature fluid of 1–11%, versus 3–16% for the East BIF and 0–16% for the West IF (Fig. 6a). It is notable that samples from the southern part of the West IF show a very low hydrothermal-fluid input based on their flat REE patterns. At Meliadine, most samples record a moderate hydrothermal influence (2–3% for the Discovery zone, 4–28% for the F-Zone, 3–22% for the Pump zone) during chert precipitation (Fig. 6b). At Musselwhite, input from the high-temperature fluid was generally low during chert formation, at 0–15% for the 4B facies, 4–7% for the 4E facies, 2–11% for the 4EA facies, and 0–5% for the 4F facies (Fig. 6c). The 4F facies samples seem to record more restricted influence by hydrothermal fluids, which is consistent with a slightly positive Eu anomaly.

The data suggest that chert geochemistry records ambient seawater and hydrothermal vent fluids for the majority of samples at all three of the studied BIF-hosted gold deposits. However, a number of samples from Pump, Discovery (sample MEL-038), and Musselwhite (samples E599656, E599660, E599665, and E599666) yield very low Y/Ho ratios associated with negative La and Y anomalies, which may represent a detrital input.

Sources and Influence of Detrital Contamination

The REE data for most chert samples from Meadowbank, Meliadine, and Musselwhite reflect the influence of seawater and some detrital contamination, as illustrated by their flat REE patterns ($Pr/Sm_{MUQ} \approx 1$) and chondritic Y/Ho ratios (i.e. Y/Ho ≈ 27). We emphasize that samples were normalized to MUQ, which we expect is a reasonable proxy for detritus during BIF deposition in the greenstone belt environment. This detrital contamination is key to understanding the depositional setting for Algoma-type BIF and thus the validity of REE+Y systematics. Therefore, to estimate the influence of the detrital component, a mixing line was calculated using the seawater composition from the North Pacific referred to above (Alibo and Nozaki, 1999) and MUQ (Kamber et al., 2005) as the two end-members (Fig. 7). The MUQ composition represents a suitable estimate of the composition of the most probable detrital contamination of cherts in Archean greenstone belts due to its basalt-dominant bimodal provenance. Prior to discussing the data in Figure 7, we note that the reason for the bulk of the samples plotting below the mixing line is due to the influence of the

high-temperature hydrothermal vent fluids input (i.e. $Pr/Sm_{MUQ} = 0.73$).

For samples from Meadowbank (Fig. 7a), the detrital influence on the REE chert chemistry is estimated at 8–100% for the Central BIF, 50–100% for the East BIF, and 30–100% for the West IF. Thus, these data indicate the East and West IF seem to record the most detrital contamination, whereas the REE composition of East and Central BIF appear to extends towards seawater compositions, which is consistent with the previous plot (Fig. 6a). All the Meadowbank samples are located either on the mixing line or below it (Fig. 7a), suggesting that detritus contributed to the chert REE signature in addition to seawater and a high-temperature hydrothermal fluid.

Some of the Meliadine samples (Fig. 7b) are distinguished by their low Y/Ho ratios, in particular the data from the Pump zone and samples MEL-025 and MEL-038 from the Discovery zone. Considering only samples located on, or directly below the mixing line, the detrital influence during chert deposition is estimated at 60–100% for Discovery, 65–100% for the F-Zone, and 85–95% at Pump. All of the F-Zone samples and most samples from Discovery (except samples MEL-025 and MEL-038) are located either on or below the mixing line, which suggests a detrital component along with variable contributions from seawater and high-temperature hydrothermal fluids (Fig. 7b).

At Musselwhite, chert samples are distinguished by their low Y/Ho ratios, especially for units 4B, 4EA, and 4F (Fig. 7c), which is similar to what is seen in some of the Meliadine samples. A detrital influence of approximately 40–100%, 80–100%, and 0–85% is estimated for units 4B, 4E, and 4EA, respectively when considering only samples located on or directly below the mixing line. According to the data, unit 4EA seems to be less affected by detrital contamination than the other facies and unit 4B shows the strongest influence of hydrothermal fluids.

The estimated influence of a detrital component as indicated above cannot be considered quantitative; however, it still indicates that for those chert samples that suggest up to 100% of MUQ contamination, there is some chemical indications of seawater influence (positive La and Y anomalies). These data, therefore, suggest chert precipitation occurred in a seawater environment associated with high-temperature hydrothermal venting fluids and some detrital input. Importantly, these data illustrate that the influence of only trace amounts of clastic detritus in the chert bands may be enough to dominate the bulk REE content and signatures of the chert.

Though the anomalous sub-chondritic Y/Ho ratios for Meliadine and Musselwhite samples are inconsistent with a detrital contamination, the ratios could indicate particle scavenging in the water column at the time of chert deposition. Scavenging may have involved Fe-oxyhydroxide minerals and may explain slightly sub-chondritic ratios for the chert bands (rather than Mn-oxyhydroxide in an Archean context; e.g. Minami et al., 1998; Bau, 1999; Kawabe et al., 1999). According to Bau (1999), Fe-oxyhydroxide precipitates, which are introduced by hydrothermal discharge in seawater, display less positive or even negative La and Y anomalies associated with a M-type lanthanide tetrad effect (Masuda et al., 1987). As a result, the association between low Y/Ho ratios and negative La and Y anomalies appears to record Fe-oxyhydroxide within the chert bands.

Influence of Fe-Oxyhydroxide Precipitation and Information about pH Precipitation

As previously suggested, some of the Meliadine and Musselwhite samples may reflect co-precipitation of chert and Fe-oxyhydroxide minerals (i.e. low Y/Ho ratio associated with negative La and Y anomalies; Bau, 1999). These Fe-oxyhydroxides may have formed under the influence of a dynamic pH shift during the mixing of alkaline hydrothermal fluids with acidic to neutral Archean seawater, which can precipitate Fe^{3+} out of Fe^{2+}-rich seawater under anoxic conditions (Shibuya et al., 2010), and/or by biological oxidation of Fe^{2+} onto the seafloor by photoautotrophic bacteria (i.e. Kappler et al., 2005; Konhauser et al., 2005). In order to explore the potential role played by Fe-oxyhydroxide minerals on chert geochemistry, mixing lines were calculated using the Alibo and Nozaki (1999) seawater composition, Fe-oxyhydroxide precipitates, and graphitic mudstone from Meliadine (the KMG unit) as end-members (Fig. 8). Fe-oxyhydroxide precipitated under experimental conditions from acidic seawater (Bau, 1999) and Fe-oxyhydroxide precipitates under experimental conditions from alkaline solutions (Kawabe et al., 1999) were selected as end-members representing a range of seawater conditions. The KMG samples are graphitic mudstone representing carbon biomass, possibly reflecting biological oxidation of Fe^{2+}.

The Meadowbank samples represent interaction of acidic seawater with Fe-oxyhydroxides (Fig. 8a), which produced the observed positive La and Y anomalies.

At Meliadine, most samples are located in the seawater domain except for the samples from the Pump deposit and samples MEL-025 and MEL-028 from the Discovery zone, which are located in the Fe-oxyhydroxide domain and thus confirm their presence in chert bands (Fig. 8b). Samples located in the seawater

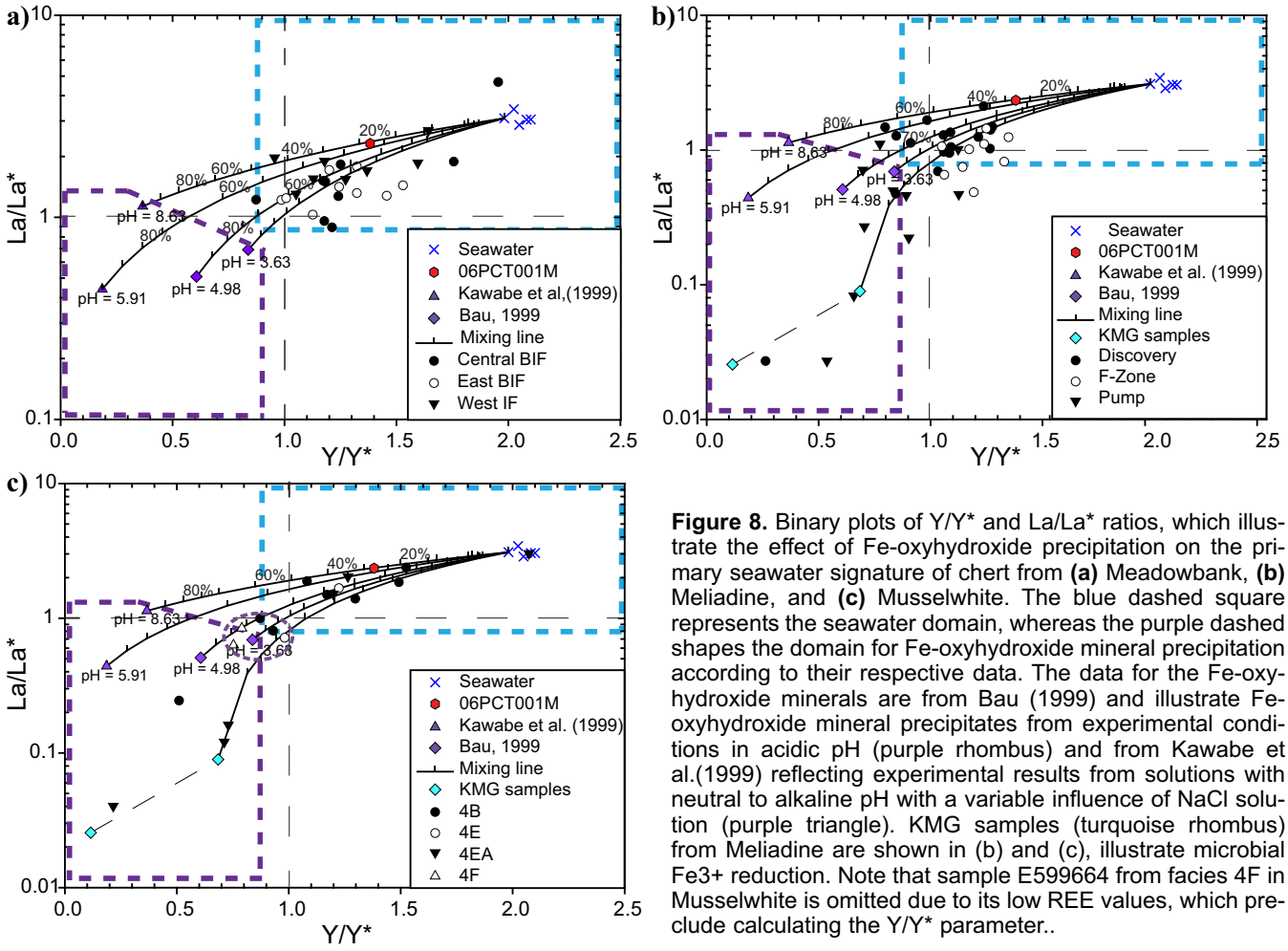

Figure 8. Binary plots of Y/Y* and La/La* ratios, which illustrate the effect of Fe-oxyhydroxide precipitation on the primary seawater signature of chert from **(a)** Meadowbank, **(b)** Meliadine, and **(c)** Musselwhite. The blue dashed square represents the seawater domain, whereas the purple dashed shapes the domain for Fe-oxyhydroxide mineral precipitation according to their respective data. The data for the Fe-oxyhydroxide minerals are from Bau (1999) and illustrate Fe-oxyhydroxide mineral precipitates from experimental conditions in acidic pH (purple rhombus) and from Kawabe et al.(1999) reflecting experimental results from solutions with neutral to alkaline pH with a variable influence of NaCl solution (purple triangle). KMG samples (turquoise rhombus) from Meliadine are shown in (b) and (c), illustrate microbial Fe3+ reduction. Note that sample E599664 from facies 4F in Musselwhite is omitted due to its low REE values, which preclude calculating the Y/Y* parameter..

domain suggest interaction of seawater and Fe-oxyhydroxide. In this deposit, two mechanisms for precipitation of Fe-oxyhydroxide are proposed: 1) influence of a dynamic pH shift between alkaline hydrothermal fluids and acidic-neutral seawater; and 2) biological oxidation of Fe^{2+}.

At Musselwhite, three groups are present. The first group reflects the interaction of seawater with Fe-oxyhydroxide and may reflect precipitation under variable pH conditions (Fig. 8c). The second group reflects precipitation of Fe-oxyhydroxide by biological oxidation (Fig. 8c). And finally, the third group could represent Fe-oxyhydroxide precipitation under acidic conditions (e.g. Bau, 1999) (Fig. 8c).

Given anoxic Archean seawater, the shale-normalized REE+Y patterns for Archean seawater will differ from modern seawater, which shows a well developed, negative Ce anomaly resulting from the oxidation of Ce^{+3} to Ce^{+4} (Planavsky et al., 2010). However, Bau (1999) experimented with the scavenging of dissolved REE+Y by precipitating Fe-oxyhydroxide at pH ranging from 3.6 to 6.2 and ambient oxygen content, and demonstrated that in the presence of Fe-oxyhydroxide, pH has a more important impact on Ce than oxygen. At pH ≤ 5, oxidative scavenging of Ce is favoured in the presence of Fe-oxyhydroxide and generates a positive Ce anomaly (Fig. 9), whereas at pH ≥ 5, the REE+Y systematics shows a negative Ce anomaly (Fig. 9).

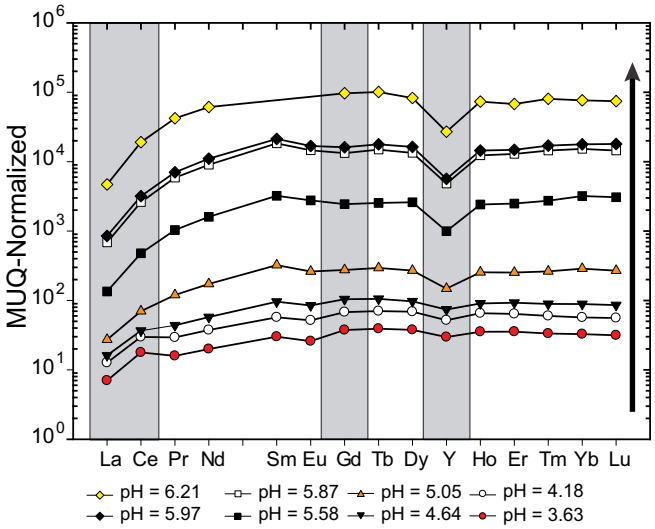

Figure 9. Plot of MUQ-normalized REE+Y patterns for experimentally produced Fe-oxyhydroxide precipitates at variable pH values (data from Bau, 1999).

Therefore, in theoretically acidic to neutral Archean seawater (e.g. Grotzinger and Kasting, 1993; Holland, 2003), the REE+Y systematics will display a weak negative Ce anomaly even in anoxic conditions.

Based on the previous statement, samples from the Pump zone, samples MEL-025, MEL-028 from the Discovery zone, and the second group of samples from Musselwhite, which may indicate interaction of Fe-oxyhydroxide from bacteria and seawater, show negative Ce anomalies that may reflect precipitation at a pH > 5, whereas most samples from the three deposits that are associated with positive Ce anomalies may reflect precipitation of Fe-oxyhydroxide at a pH < 5.

IMPLICATIONS FOR EXPLORATION

Based on the results and conclusions summarized herein, it does not appear that the primary depositional setting of the BIFs is a key ingredient for gold mineralization. This conclusion likely relates to the fact that the gold mineralization in each of these deposits occurs as part of an epigenetic event(s) during regional orogenesis; instead the dominant factor for such BIF-hosted gold deposits is the Fe-rich nature of the host, which is similar in all the BIF settings studied. However, our systematic sampling outward from the gold zones at all three deposits should provide a hydrothermal footprint in the chert chemistry, which will be defined in future stages of this project. These latter data can then be used to evaluate the influence of gold mineralizing fluids in Algoma-type BIFs.

FUTURE WORK

In the near future, the KMG samples will be analysed for their $\delta^{13}C$ signature, which will provide more insight into their nature of formation and origin. Furthermore, chert samples from the Beardmore-Geraldton gold deposit area and some additional samples from Musselwhite deposit will be analysed and interpreted in the same manner as the other samples above and a depositional setting will be defined. Moreover, a potential hydrothermal footprint at both the regional- and macroscopic-scale will also be defined where feasible (i.e. respectively at Beardmore-Geraldton and Meliadine).

ACKNOWLEDGEMENTS

The study is supported by both TGI-4 funding from Natural Resources Canada and funding through a Natural Sciences and Engineering Research Council Collaborative Research and Development agreement with participation by Agnico Eagle Mines Ltd. and Goldcorp. The authors also thank Drs. M. Leybourne, C. Lawley, and S. Pehrsson for discussions regarding the geochemistry and regional geological setting of the study areas, respectively. The LA-ICP-MS analyses were done in the Geochemical Fingerprinting Laboratory at Laurentian University with the capable assistance of Dr. J. Petrus. Finally, we sincerely acknowledge the contribution of Drs. B. Dubé, S. Castonguay, and P. Mercier-Langevin of the Geological Survey of Canada for their input and continued support.

REFERENCES

Alexander, B.W., Bau, M., Andersson, P., and Dulski, P., 2008. Continentally-derived solutes in shallow Archean sea water; rare earth element and Nd isotope evidence in iron formation from the 2.9 Ga Pongola Supergroup, South Africa; Geochimica et Cosmochimica Acta, v. 72, p. 378–394.

Alibo, D.S. and Nozaki, Y., 1999. Rare earth elements in seawater: particle association, shale-normalization, and Ce oxidation; Geochimica et Cosmochimica Acta, v. 63, p. 363–372.

Allwood, A.C., Kamber, B.S., Walter, M.R., Burch, I.W., and Kanik, I., 2010. Trace element record depositional history of an Early Archean stromatolitic carbonate platform; Chemical Geology, v. 270, p. 148–163.

Bau, M., 1999. Scavenging of dissolved yttrium and rare-earths by precipitating iron-oxyhydroxide: Experimental evidence for Ce oxidation, Y-Ho fractionation, and lanthanide tetrad effect; Geochimica et Cosmochimica Acta, v. 63, no. 1, p.67–77.

Bau, M. and Dulski, P., 1996. Distribution of Y and rare-earth elements in the Penge and Kuruman Iron Formations, Transvaal Supergroup, South Africa; Precambrian Research, v. 79, p. 37–55.

Bekker, A., Slack, J.F., Planavsky, N., Krapez, B., Hofmann, A., Konhauser, K.O., and Rouxel, J., 2010. Iron formation: the sedimentary product of a complex interplay among mantle, tectonic, oceanic and biospheric processes; Economic Geology, v. 105, p. 467–508.

Bolhar, R., Van Kranendonk, M.J., and Kamber, B.S., 2005. A trace element study of siderite-jasper banded iron formation in the 3.45 Ga Warrawoona Group, Pilbara craton-Formation from hydrothermal fluids and shallow seawater; Precambrian Research, v. 137, p. 93–114.

Danielson, A., Moeller, P., and Dulski, P., 1992. The europium anomalies in banded iron formations and the thermal history of the oceanic crust; Chemical Geology, v. 97, p. 89–100.

Goodwin, A.M., 1973. Archean iron-formations and tectonic basins of the Canadian Shield; Economic Geology, v. 68, p. 915–933.

Gourcerol, B., Thurston, P.C., Kontak, D.J., and Côté-Mantha, O., 2014. Interpretations and implications of preliminary LA ICP-MS analysis of chert for the origin of geochemical signatures in banded iron formations (BIFs) from the Meadowbank gold deposit, Western Churchill Province, Nunavut; Geological Survey of Canada, Current Research 2014-1, 26 p.

Gourcerol, B., Thurston, P.C., Kontak, D.J., Côté-Mantha, O., and Biczok, J., 2015. Distinguishing primary and mineralization-related signatures of chert from the banded iron formation-type gold deposits at Musselwhite, Ontario and Meadowbank, Nunavut; Geological Survey of Canada, Current Research 2015-1, 21 p.

Grotzinger, J.P. and Kasting, J.F., 1993. New constraints on Precambrian ocean composition; Journal of Geology, v. 101, p. 235–243.

Hanor, J.S. and Duchac, K.C., 1990. Isovolumetric silicification of early Archean komatiites; geochemical mass balances and constraints on origin; Journal of Geology, v. 98, p. 863–877.

Holland, H.D., 2003. The geologic history of seawater, *In:* Treatise on Geochemistry, (ed.) H.D. Holland and K.K. Turekian; Pergamon, Oxford, p. 583–625.

Kamber, B.S. and Webb, G.E., 2007. Transition metal abundances in microbial carbonate: a pilot study based on in situ LA-ICP-MS analysis; Geobiology, v. 5, p. 375–389.

Kamber, B.S., Bolhar, R., and Webb, G.E., 2004. Geochemistry of late Archean stromatolites from Zimbabwe: evidence for microbial life in restricted epicontinental seas; Precambrian Research, v. 132, p. 379–399.

Kamber, B.S., Greig, A., and Collerson, K.D., 2005. A new estimate for the composition of weathered young upper continental crust from alluvial sediments, Queensland, Australia; Geochimica et Cosmochimica Acta, v. 69, p. 1041–1058.

Kappler, A., Pasquero, C., Konhauser, K.O., and Newman D.K.,2005, Deposition of banded iron formations by anoxygenic phototrophic Fe(II)-oxidizing bacteria: Geology, v. 33, p. 865–868.

Kawabe, I., Ohta, A., Ishii, S., Tokumura, M., and Miyauchi, K., 1999. REE partitioning between Fe–Mn oxyhydroxide precipitates and weakly acid NaCl solutions: Convex tetrad effect and fractionation of Y and Sc from heavy lanthanides; Geochemical Journal, v. 33, p. 167–179.

Konhauser, O.K., Newman, D.K., and Kappler, A., 2005. The potential significance of microbial Fe(III) reduction during deposition of Precambrian banded iron formations; Geobiology, v. 3, p. 167–177.

Lawrence, M.G. and Kamber, B.S., 2006. The behavior of the rare earth elements during estuarine mixing- revisited; Marine Chemistry, v. 100, p.147–161.

Masuda, A., Kawakami, O., Dohmoto, Y., and Takenaka, T., 1987. Lanthanide tetrad effects in nature: two mutually opposite types, W and M; Geochemical Journal, v. 21, p. 119–124.

Minami, M., Masuda, A., Takahashi, K., Adachi, M., and Shimizu, H., 1998. Y-Ho fractionation and lanthanide tetrad effect observed in cherts; Geochemical Journal, v. 32, p. 405–419.

Ohmoto, H., Watanabe, Y., Yamaguchi, K.E., Naraoka, H., Haruna, M., Kakegawa, T., Hayashi, K., and Kato, Y., 2006. Chemical and biological evolution of early Earth: Constraints from banded iron formations; Geological Society of America Memoir, v. 198, p. 291−331.

Planavsky, N., Bekker, A., Rouxel, O.J., Kamber, B.S., Hofmann, A.W., Knudsen, A., and Lyons, T.W., 2010. Rare earth element and yttrium compositions of Archean and Paleoproterozoic Fe formations revisited: new perspectives on the significance and mechanisms of deposition; Geochimica et Cosmochimica Acta, v. 74, p. 6387–6405.

Shibuya, T., Komiya, T., Nakamura, K., Takai, K., and Maruyama, S., 2010. Highly alkaline, high-temperature hydrothermal fluids in the early Archean ocean; Precambrian Research, v. 182, p. 230–238.

Thurston, P.C., Kamber, B.S., and Whitehouse, M., 2011. Archean cherts in banded iron formation: Insight into Neoarchean ocean chemistry and depositional processes; Precambrian Research, v. 214-215, p. 227–257.

Veizer, J., 1988, The evolving exogenic cycle, *In:* Chemical Cycles in the Evolution of the Earth, (ed.) B.C. Gregor, R.M. Garrels, F.T. Mackenzie, and B.J. Maynard; Wiley-Interscience, New York, p. 175–218.

Wheeler, J.O., Hoffman, P.F., Card, K.D., Davidson, A., Sanford, B.V., Okulitch, A.V., and Roest, W.R., 1996. Geological map of Canada; Geological Survey of Canada, Map 1860A, CD-ROM.